Control and performance of a flywheel energy storage system based on a doubly-fed induction generator-motor for power conditioning

Hirofumi Akagi
Okayama University

Hikaru Sato
Okayama University

Control and Performance of a Flywheel Energy Storage System Based on a Doubly-Fed Induction Generator-Motor for Power Conditioning

Hirofumi Akagi, *Fellow, IEEE*
Department of Electrical Engineering
Okayama University
Okayama-city, 700-8530, JAPAN

Hikaru Sato
PS Division, Accelerator Department
High-Energy Accelerator Research Organization
KEK, Tsukuba-city, 305-0801, JAPAN

Abstract— A flywheel energy storage system based on a doubly-fed induction generator-motor basically consists of a wound-rotor induction machine and a cycloconverter or a voltage-source PWM rectifier-inverter which is used as an ac exciter. Adjusting the rotor speed makes the generator-motor either release the kinetic energy to the power system or absorb it from the utility grid. Thus, the generator-motor has the capability of achieving not only reactive power control, but also active power control based on the flywheel effect of the rotating parts. This paper proposes a new control strategy for a doubly-fed induction generator-motor, which is characterized by the combination of vector control and decoupling control. The control strategy enables the induction generator-motor to perform active power control independent of reactive power control even in transient states. The validity of the theory developed in this paper, along with the effectiveness and viability of the control strategy, is confirmed by computer simulation. In addition, this paper discusses a transient behavior of a magnetizing current in the induction machine.

I. INTRODUCTION

A. Background

The next generation of proton synchrotrons, which is being designed by the High-Energy Accelerator Research Organization in Japan, requires a high-accuracy large-capacity magnet power supply rated at 50-70 MW. Fig. 1 shows an operating pattern of the magnet power supply, which has a repetitive period as short as 4 sec. The pattern is divided by the following four periods: a flat base period for beam injection, a current-increasing period for beam acceleration, a flat top period for accelerated beam extraction, and a current-decreasing period for releasing electromagnetic energy from the ring magnet [1]. The active power drawn from the utility grid drastically changes in a range from +55 MW to −55 MW within 4 sec. This fluctuation in active power may produce serious effects on power systems which are upstream and downstream of the installation site of the magnet power supply. Hence, installation of a large-capacity energy storage system to the magnet power supply is now under consideration, aiming at load-leveling over a repetitive period as short as 4 sec.

Attention has been paid to a flywheel energy storage system based on a doubly-fed induction generator-motor for the purpose of power conditioning. It is also referred to as an "adjustable-speed rotary condenser" capable of both active power control and reactive power control, in con-
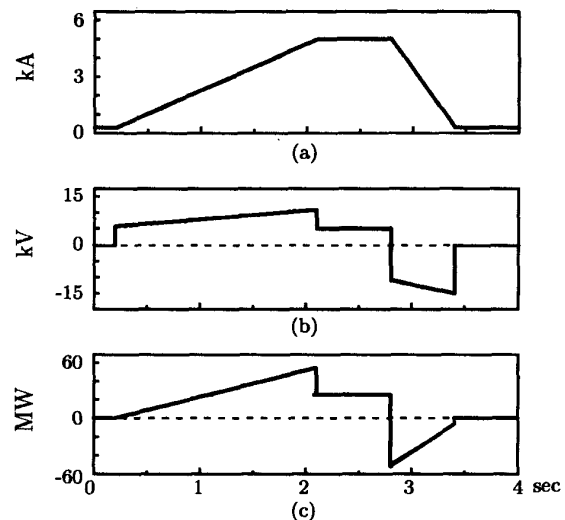

Fig. 1. Operating pattern of a magnetic power supply for a proton synchrotron. (a) Magnet current. (b) Magnet voltage. (c) Active power.

trast with a conventional "synchronous-speed rotary condenser" capable of only reactive power control. The secondary (rotor) windings of the doubly-fed induction machine are excited by three-phase low-frequency ac currents, which are supplied via slip rings by either a cycloconverter or a voltage-fed PWM rectifier-inverter. The ac excitation on the basis of a rotor-position feedback loop makes it possible to achieve stable variable-speed operation. Adjusting the rotor speed makes the generator-motor either release the electric power to the utility grid or absorb it from the utility grid. Therefore, the flywheel energy storage system is more suitable for repetitively absorbing and releasing electric energy for a short period of time than a battery energy storage system [2]. The required capacity of power electronic equipment for ac excitation is in a range from one-fifth to one-seventh as small as the capacity of the wound-rotor induction machine. Thus the flywheel energy storage system is superior in practicability and viability to a superconductive magnetic energy storage (SMES) system. Although a feasible study of an extremely large-capacity SMES rated at 400-MW and 20-MWh was

performed [3][4], it would take a long period of time to put large-capacity SMES systems into practical use.

B. The 200-MJ Flywheel Energy Storage System

The 200-MJ flywheel energy storage system based on a doubly-fed induction machine for line-frequency regulation on a 132-kV bus has been installed and was commissioned in August of 1996 at the Chujowan substation of the Okinawa Electric Power Company in Japan [5]. It consists of a 26.5-MVA wound-rotor induction machine coupled with a flywheel of 74,000 kg with a 4-m diameter, a 6.55-MVA three-phase twelve-pulse line-commutated cycloconverter, an excitation transformer and a controller. This flywheel energy storage system could be referred to as ROTES (ROTary Energy Storage)[5]. The rotor windings of the 12-pole induction machine are excited by three-phase low-frequency ac currents which are supplied via slip rings by the cycloconverter. The stator terminals rated at 6.6 kV are connected to the 66-kV, 60-Hz utility grid through a step-up transformer. The output frequency of the cycloconverter is controlled within 0.25–9.0 Hz, and the line frequency is 60 Hz. This enables the cycloconverter to operate in a *circulating current-free* mode. The generator-motor with a synchronous speed of 600 rpm is adjusted in a speed range from −15% (510 rpm) to +15% (690 rpm). The electric energy is stored as the rotating kinetic energy with a flywheel effect of $GD^2 = 710$ t-m^2. The ROTES has been operating properly for more than one year, showing great promise as a FACTS device which has the capability of releasing or absorbing electric energy with a response time as fast as 100 ms. However, reference [5] makes no detailed description of the control strategy for the ROTES.

C. Control Strategy

A 40-MJ flywheel energy storage system based on a 70-MVA doubly-fed induction machine should be installed on the ac side of the magnet power supply shown in Fig. 1, in order to achieve perfect load-leveling. Comparison with the 200-MJ system installed for line-frequency regulation leads to the possibility that the 40-MJ system does not need to couple any flywheel with the rotor, because the induction machine rating required to the 40-MJ system is 2.6 times as large as that required to the 200-MJ system. On the contrary, the 40-MJ system needs to achieve much faster charge/discharge of active power than the 200-MJ system. Little literature has been published on control strategy and dynamic performance of doubly-fed wound-rotor induction machines [6]-[9]. In his book [6], Leonhard describes a control strategy for an adjustable-speed doubly-fed induction machine, intended for independent control of active power and reactive power. The control strategy provides two kinds of current controllers: inner feedback loops of the secondary (rotor) currents on the d-q coordinates and outer feedback loops of the primary (stator) currents on the γ-δ coordinates. However, it is not clarified theoretically why the control strategy requires the two kinds of current controllers.
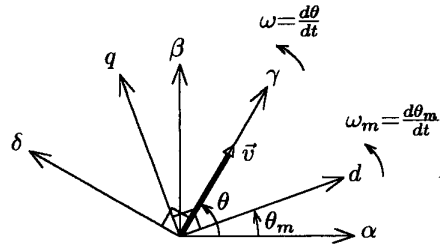

Fig. 2. Stationary and rotating coordinates

This paper proposes a new control strategy for an adjustable-speed doubly-fed induction machine acting as a flywheel energy storage system. The control strategy is characterized by constituting direct feedback control loops of the primary (stator) currents on the γ-δ coordinates, but without inner feedback control loops of the secondary (rotor) currents on the d-q coordinates, with the help of decoupling control based on feedforward compensation. The validity of the theory developed in this paper, along with the effectiveness and viability of the control strategy, is confirmed by computer simulations using a general-purpose software package referred to as EMTDC. In addition, this paper discusses a transient behavior of a magnetizing current in the doubly-fed induction machine.

II. SYSTEM CONFIGURATION

A flywheel energy storage system based on a doubly-fed induction machine will be installed in the vicinity of a large-capacity load such as in Fig. 1, which is accompanied by significant fluctuation of active power. The first purpose of the energy storage system is to achieve load-leveling over the repetitive period of time. The second purpose is to perform reactive power compensation of the load, rather than to improve voltage stability in power systems. In the following analysis and simulation, the power system upstream of installation site of the energy storage system is assumed to be an infinite bus with three-phase balanced sinusoidal voltage. Moreover, the doubly-fed induction generator-motor is assumed to be a two-phase two-pole machine for the sake of simplicity

A. Stationary and Rotating Coordinates

Fig. 2 shows stationary and rotating coordinates applied to the analysis in this paper. The α-β coordinates are stationary on the stator. The d-q coordinates are rotating at an angular velocity of $\omega = d\theta_m/dt$, synchronized with the rotor speed, where θ_m is the rotor position. The γ-δ coordinates are rotating at an angular velocity of $\omega = d\theta/dt$, where θ means the line phase. Because the primary voltage vector $\vec{v_1}$ is aligned with the γ axis, as shown in Fig. 2, the primary currents $i_{\gamma 1}$ and $i_{\delta 1}$ correspond to the instantaneous active and reactive currents i_p and i_q, that is, $i_p = i_{\gamma 1}$ and $i_q = i_{\delta 1}$[10].
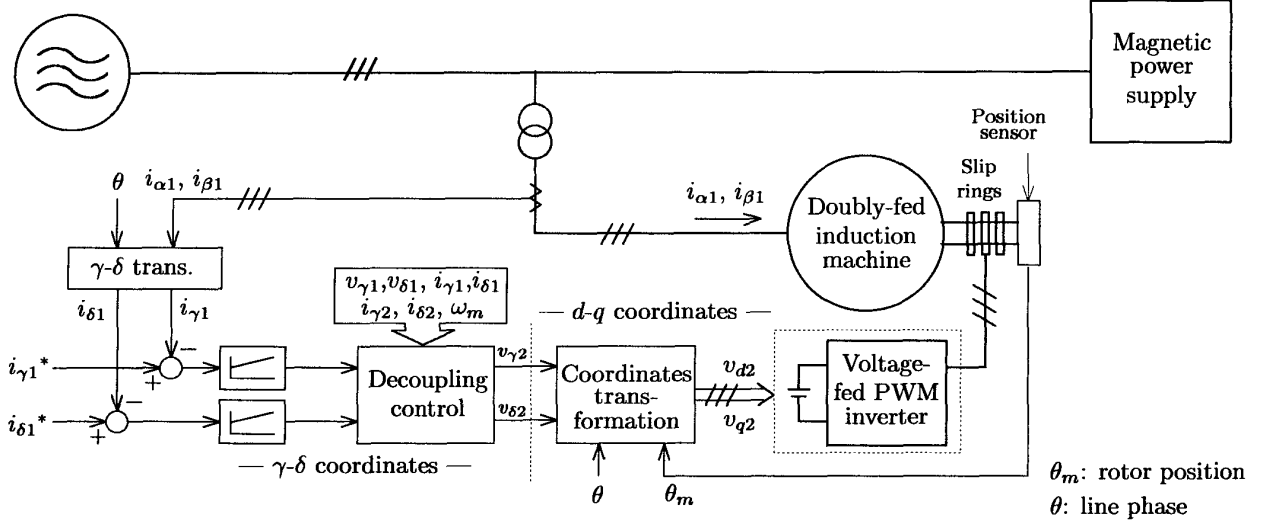
33

Fig. 3. System configuration of the doubly-fed flywheel generator-motor.

B. System Configuration

Fig. 3 depicts the system configuration of the flywheel energy storage system based on the doubly-fed induction machine, and Table 1 summarizes its machine constants. The generator-motor itself has the same structure as a wound-rotor induction machine equipped with slip rings. The primary windings are connected to the utility grid, while the secondary windings are connected to the ac terminals of a voltage-fed PWM inverter operating as an ac exciter.

The control circuit detects the primary currents $i_{\alpha 1}$ and $i_{\beta 1}$ on the α-β coordinates and then transforms them into the primary currents $i_{\gamma 1}$ and $i_{\delta 1}$ on the γ-δ coordinates, on the basis of the detected line phase θ. Comparison of $i_{\gamma 1}$ and $i_{\delta 1}$ with their references $i_{\gamma 1}{}^*$ and $i_{\delta 1}{}^*$, and proportional-plus-integral (PI) control constitute two feedback loops. It is also easy to detect the primary voltages and the secondary currents in the wound-rotor induction machine. These detected voltages and currents are transformed into those on the γ-δ coordinates with the help of θ and θ_m. Decoupling control discussed in the next section makes it possible to achieve instantaneous active power control independent of instantaneous reactive power control even in transient states. The decoupling control based on feedforward control is characterized by using the detectable voltages, currents and rotor position in addition to the machine parameters. The following equation transforms the secondary voltage references on the γ-δ coordinates, $v_{\gamma 2}$ and $v_{\delta 2}$ into those on the d-q coordinates, v_{d2} and v_{q2},

$$\begin{bmatrix} v_{d2} \\ v_{q2} \end{bmatrix} = \begin{bmatrix} \cos(\theta - \theta_m) & -\sin(\theta - \theta_m) \\ \sin(\theta - \theta_m) & \cos(\theta - \theta_m) \end{bmatrix} \begin{bmatrix} v_{\gamma 2} \\ v_{\delta 2} \end{bmatrix}. \quad (1)$$

Note that the PWM pattern of the voltage-fed inverter is directly determined from v_{d2} and v_{q2}. Such a dc voltage source as shown in Fig. 3 will be implemented with a

voltage-fed PWM rectifier in a real system. When the ac terminals of the PWM rectifier are connected to the primary terminals of the induction machine, a small amount of power flow exists between the ac terminals and the primary terminals. For the sake of simplicity, the power flow is neglected from the following analysis. In addition, the PWM inverter in Fig. 3 is replaced by two sets of controllable ac-voltage sources.

C. Modeling for Simulation

The EMTDC supports only two machines models: a salient-pole synchronous machine and a squirrel-cage induction machine. Therefore, the authors have created a wound-rotor induction machine model by making use of the model-building function. The constructed induction machine model on the d-q coordinates consists of a set of voltage-current differential equations, the torque equation and the mechanical dynamic equation. The standard mod-

34

els supported by the EMTDC are used to simulate six GTO thyristors and diodes in the three-phase voltage-fed PWM inverter.

III. CONTROL STRATEGY

A. Combination of Vector Control and Decoupling Control

In general, a set of voltage-current differential equations of a two-pole wound-rotor induction machine on the γ-δ coordinates is given by

$$
\begin{bmatrix} v_{\gamma 1} \\ v_{\delta 1} \\ v_{\gamma 2} \\ v_{\delta 2} \end{bmatrix} = \begin{bmatrix} r_1 + \frac{d}{dt}L_1 & -\omega L_1 \\ \omega L_1 & r_1 + \frac{d}{dt}L_1 \\ \frac{d}{dt}M & -(\omega - \omega_m)M \\ (\omega - \omega_m)M & \frac{d}{dt}M \end{bmatrix}
$$

$$
\begin{bmatrix} \frac{d}{dt}M & -\omega M \\ \omega M & \frac{d}{dt}M \\ r_2 + \frac{d}{dt}L_2 & -(\omega - \omega_m)L_2 \\ (\omega - \omega_m)L_2 & r_2 + \frac{d}{dt}L_2 \end{bmatrix} \begin{bmatrix} i_{\gamma 1} \\ i_{\delta 1} \\ i_{\gamma 2} \\ i_{\delta 2} \end{bmatrix}. \quad (2)
$$

Eliminating $di_{\gamma 2}/dt$ from the first and third rows, and $di_{\delta 2}/dt$ from the second and fourth rows of (2) yields the following equations:

$$
\begin{bmatrix} l\frac{d}{dt}i_{\gamma 1} \\ l\frac{d}{dt}i_{\delta 1} \end{bmatrix} = \begin{bmatrix} \frac{L_2}{M}v_{\gamma 1} - \frac{L_2 r_1}{M}i_{\gamma 1} + r_2 i_{\gamma 2} \\ \frac{L_2}{M}v_{\delta 1} - \frac{L_2 r_1}{M}i_{\delta 1} + r_2 i_{\delta 2} \end{bmatrix}
$$

$$
\begin{matrix} +l\omega i_{\delta 1} + \omega_m(Mi_{\delta 1} + L_2 i_{\delta 2}) - v_{\gamma 2} \\ -l\omega i_{\gamma 1} - \omega_m(Mi_{\gamma 1} + L_2 i_{\gamma 2}) - v_{\delta 2} \end{matrix} \quad (3)
$$

$$
l = (L_1 L_2 - M^2)/M. \quad (4)
$$

The state variables $i_{\gamma 1}$ and $i_{\delta 1}$ can be considered as the output variables of the system, while the input variables $v_{\gamma 2}$ and $v_{\delta 2}$ are given by

$$
\begin{bmatrix} v_{\gamma 2} \\ v_{\delta 2} \end{bmatrix} = \begin{bmatrix} \frac{L_2}{M}v_{\gamma 1} - \frac{L_2 r_1}{M}i_{\gamma 1} + r_2 i_{\gamma 2} + l\omega i_{\delta 1} \\ \frac{L_2}{M}v_{\delta 1} - \frac{L_2 r_1}{M}i_{\delta 1} + r_2 i_{\delta 2} - l\omega i_{\gamma 1} \end{bmatrix}
$$

$$
\begin{matrix} +\omega_m(Mi_{\delta 1} + L_2 i_{\delta 2}) - K(i_{\gamma 1}^* - i_{\gamma 1}) \\ -\omega_m(Mi_{\gamma 1} + L_2 i_{\gamma 2}) - K(i_{\delta 1}^* - i_{\delta 1}) \end{matrix} \quad (5)
$$

The first to fifth terms on the right side of (5) are the so-called "cross-coupling" terms, which contribute to interference between the γ-axis and the δ-axis. Fortunately, the "cross-coupling" terms can be calculated from the primary voltages, the primary and secondary currents, and the angular velocity of the rotor—all of which are easily detectable—as well as the machine parameters. Hence, decoupling control based on feedforward control is applicable to (5), intended for compensation of the interference. The sixth terms on the γ- and δ-axes constitute the so-called "feedback loops," respectively. The terms make $i_{\gamma 1}$ and $i_{\delta 1}$ follow their references on the γ- and δ-axes, where K is a proportional gain. Substitution of $v_{\gamma 2}$ and $v_{\delta 2}$ given by (5) into (3) produces

$$
\begin{bmatrix} \frac{d}{dt}i_{\gamma 1} \\ \frac{d}{dt}i_{\delta 1} \end{bmatrix} = \frac{K}{l} \begin{bmatrix} (i_{\gamma 1}^* - i_{\gamma 1}) \\ (i_{\delta 1}^* - i_{\delta 1}) \end{bmatrix}. \quad (6)
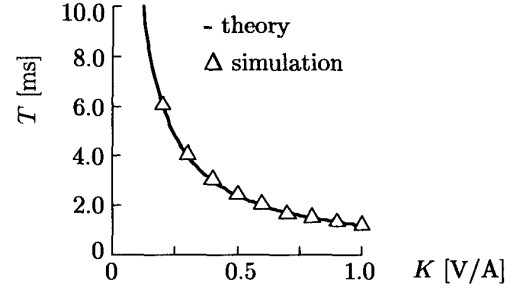$$

Fig. 4. Feedback gain and time constant.

The Laplace transformation of (6) is represented as follows:

$$
\begin{bmatrix} I_{\gamma 1}(s) \\ I_{\delta 1}(s) \end{bmatrix} = \begin{bmatrix} \frac{1}{1 + sT}I_{\gamma 1}^*(s) \\ \frac{1}{1 + sT}I_{\delta 1}^*(s) \end{bmatrix}. \quad (7)
$$

The above equation implies that the control system is no longer a complex high-order system, but a simple first-order system exhibiting no cross-coupling between the γ- and δ-axes. As a result, the time constant of $i_{\gamma 1}$ and $i_{\delta 1}$, T is given by

$$
T = l/K. \quad (8)
$$

The control strategy based on (5) is characterized by excluding any differential term.

B. Verification by Simulation

Computer simulation using the EMTDC was performed to verify the validity of the theory developed in this section. Here, the three-phase voltage-fed PWM inverter is assumed to be two-phase ideal voltage sources. Fig. 4 shows the time constant of i_p with respect to a step change in i_p^* under $i_q^* = 0$, as a function of K. The simulated results agree well with the theoretical results, and T is in inverse-proportion to K.

C. Effects of Disagreement between Machine Parameters and Control Constants

Disagreement between machine parameters and control constants results in unsatisfactory feedforward compensation, thus leading to imperfect decoupling control. For instance, saturation and nonlinearity of iron core, as well as temperature-dependence of resistors, may cause variations of inductances and resistances in the induction machine. Moreover, errors in measurement of the machine parameters may induce disagreement. When a feedback loop with only a proportional gain is integrated into the control system, the disagreement produces steady-state errors in the primary currents i_p and i_q. The effect of the disagreement on the steady-state errors is shown by computer simulation under the conditions that the mutual inductance M varies while the leakage inductances of the primary and secondary
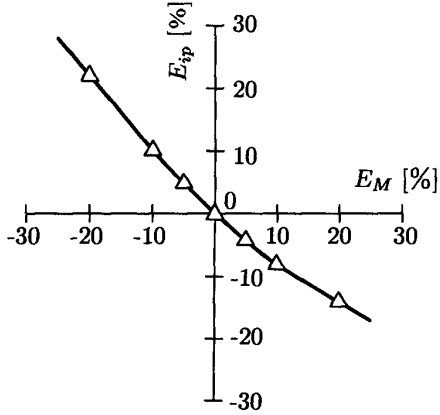
35

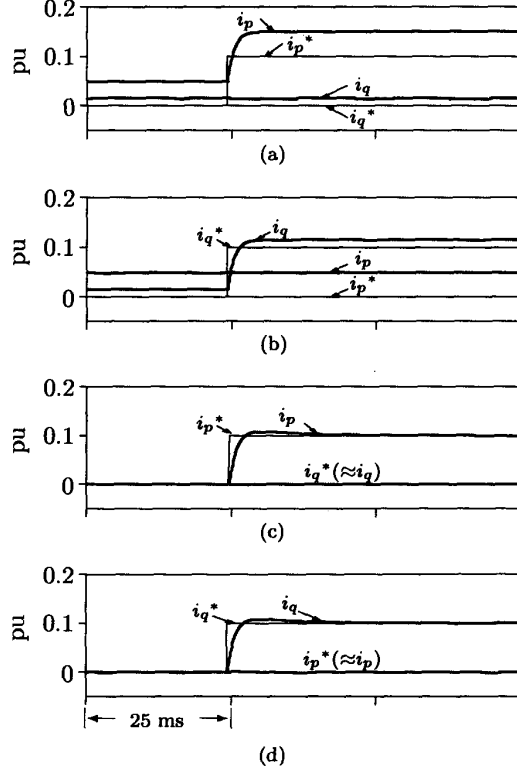Fig. 5. Mutual inductance and steady-state errors.

Fig. 6. Simulated waveforms when the mutual inductance decreases by 5 %. (a) Step response of $i_p{}^*$ under $i_q{}^* = 0$ in the case of the P controller. (b) Step response of $i_q{}^*$ under $i_p{}^* = 0$ in the case of the P controller. (c) Step response of $i_p{}^*$ under $i_q{}^* = 0$ in the case of the PI controller. (d) Step response of $i_q{}^*$ under $i_p{}^* = 0$ in the case of the PI controller.

windings do not. Fig. 5 shows relationships between errors in M and steady-state errors in i_p, with a proportional gain of $K_P = 1$ [V/A]. Here, E_M [%] is the ratio of the error to the nominal value, and E_{ip} [%] is the ratio of the steady-state error to the rated current. Fig. 5 suggests that the disagreement of the mutual inductance is accompanied by non-negligible steady-state errors. However, a disagreement of the secondary resistance by 20% induces a steady-state error as small as about 1%, which is not so serious as the disagreement of the mutual inductance.

D. Compensation for Steady-State Errors

A proportional-plus-integral controller (PI controller) is introduced to compensate for the steady-state errors caused by the disagreement pointed out in the above subsection. Fig. 6 shows simulated waveforms for a step change in $i_p{}^*$ under $i_q{}^* = 0$, when the mutual inductance in the induction machine is decreased by 5% without any change in the control constants. Here, the proportional gain in the P controller is designed as $K_P = 1$ [V/A], while the PI controller is designed as follows: the proportional gain $K_P = 1$ [V/A], and the time constant $T_I = 10$ ms. Serious steady-state errors i_p and i_q occur in (a) and (b), whereas no steady-state errors appear in (c) and (d).

IV. DISCUSSION ON MAGNETIZING CURRENTS

A. Derivation of an Equivalent Circuit

When voltage vectors and current vectors are introduced, the voltage-current differential equation of the induction machine on the α-β coordinates is given by

$$\begin{bmatrix} \vec{v}_1 \\ \vec{v}_2 \end{bmatrix} = \begin{bmatrix} r_1 + \frac{d}{dt}L_1 & \frac{d}{dt}M \\ \frac{d}{dt}M - \vec{J}\omega_m M & r_2 + \frac{d}{dt}L_2 - \vec{J}\omega_m L_2 \end{bmatrix} \begin{bmatrix} \vec{i}_1 \\ \vec{i}_2 \end{bmatrix}$$

$$(9)$$

where

$$\vec{v}_1 = [v_{\alpha 1}, \ v_{\beta 1}]^t, \quad \vec{v}_2 = [v_{\alpha 2}, \ v_{\beta 2}]^t,$$

$$\vec{i}_1 = [i_{\alpha 1}, \ i_{\beta 1}]^t, \quad \vec{i}_2 = [i_{\alpha 2}, \ i_{\beta 2}]^t,$$

and

$$\vec{J} = \begin{bmatrix} 0 & -1 \\ 1 & 0 \end{bmatrix}.$$

The second row on the right side of (9) is written down as follows:

$$\vec{v}_2 = \frac{d}{dt}M\vec{i}_1 + \frac{d}{dt}L_2\vec{i}_2 + r_2\vec{i}_2 - \vec{J}\omega_m \times (M\vec{i}_1 + L_2\vec{i}_2). \quad (10)$$

The fourth term on the right side of the above equation corresponds to the so-called "electromotive force," which is represented by $\vec{v}_e$ as follows:

$$\vec{v}_e = -\vec{J}\omega_m \times (M\vec{i}_1 + L_2\vec{i}_2), \quad (11)$$

where $\times$ is a vector product. New voltage and current vectors $\vec{v}_2{}'$ and $\vec{i}_2{}'$ are defined by

$$\vec{v}_2{}' = \frac{L_1}{M}(\vec{v}_2 - \vec{v}_e - r_2\vec{i}_2) \quad (12)$$
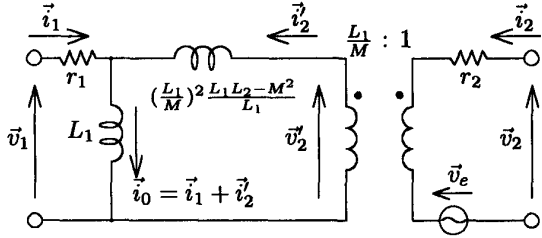
36

Fig. 7. Equivalent circuit for the wound-rotor induction machine, with the focus on the total linkage flux of the primary windings.

$$\vec{i_2}' = \frac{M}{L_1}\vec{i_2}. \tag{13}$$

Substitution of the above equations to (9) yields

$$\vec{v_1} = L_1\frac{d}{dt}(\vec{i_1} + \vec{i_2}') + r_1\vec{i_1} \tag{14}$$

$$L_1\frac{d}{dt}(\vec{i_1} + \vec{i_2}') - \vec{v_2}' = (\frac{L_1}{M})^2\frac{L_1L_2 - M^2}{L_1}\frac{d}{dt}\vec{i_2}' \tag{15}$$

$$\vec{v_2}' = L_1\frac{d}{dt}\vec{i_1} + (\frac{L_1}{M})^2 L_2\frac{d}{dt}\vec{i_2}'. \tag{16}$$

Fig. 7 depicts the equivalent circuit derived from (9)–(16), which is characterized by applicability to analysis in transient states. The primary and the secondary in the equivalent circuit are coupled by an ideal transformer with a turn ratio of L_1/M : 1. Note that $(L_1/M)^2(L_1L_2 - M^2)/L_1$ is the sum of both the leakage inductance in the primary and that in the secondary, which is referred to the primary. In Fig. 7, $\vec{i_0}$ is a magnetizing current vector corresponding to the total linkage flux in the primary, which will be discussed in the following subsection.

B. Discussion on a Magnetizing Current Vector $\vec{i_0}$

In this subsection, the primary and secondary resistances r_1 and r_2 are disregarded for the sake of simplicity. The primary and secondary interlinkage flux vectors, $\vec{\phi_1}$ and $\vec{\phi_2}$ are given by

$$\begin{bmatrix} \vec{\phi_1} \\ \vec{\phi_2} \end{bmatrix} = \begin{bmatrix} L_1 & M \\ M & L_2 \end{bmatrix} \begin{bmatrix} \vec{i_1} \\ \vec{i_2} \end{bmatrix}. \tag{17}$$

Equation (17) gives $\vec{\phi_1}$ as follows:

$$\vec{\phi_1} = L_1\vec{i_1} + M\vec{i_2}. \tag{18}$$

Substitution of (13) to (18) produces

$$\vec{\phi_1} = L_1(\vec{i_1} + \vec{i_2}') = L_1\vec{i_0}. \tag{19}$$

The above equation implies that $\vec{i_0}$ is a magnetizing current vector corresponding to the primary interlinkage flux vector[12]. The primary voltage vector $\vec{v_1}$ is given by

$$\vec{v_1} = \frac{d}{dt}\vec{\phi_1} = L_1\frac{d}{dt}\vec{i_0}. \tag{20}$$

This means that $\vec{i_0}$ is determined by $\vec{v_1}$ when L_1 is a constant value.
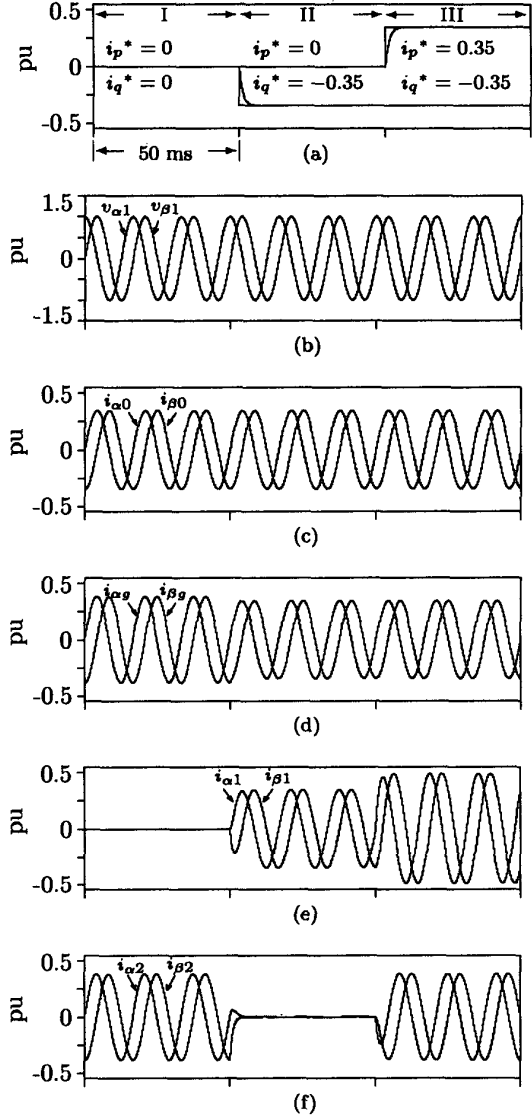

Fig. 8. Voltage and current waveforms on the α-β coordinates in transient states: (a) Instantaneous active and reactive currents, i_p and i_q. (b) Primary voltages, $v_{\alpha 1}$ and $v_{\beta 1}$. (c) Magnetizing currents equivalent to the primary flux, $i_{\alpha 0}$ and $i_{\beta 0}$. (d) Magnetizing currents equivalent to the gap flux, $i_{\alpha g}$ and $i_{\beta g}$. (e) Primary currents, $i_{\alpha 1}$ and $i_{\beta 1}$. (f) Secondary currents, $i_{\alpha 2}$ and $i_{\beta 2}$.

C. Relationship between the Primary Flux Vector and the Gap Flux Vector

Let the primary leakage inductance of the induction machine be l_1. The following relationship between $\vec{\phi_1}$ and $\vec{\phi_g}$ exists:

$$\vec{\phi_1} = l_1\vec{i_1} + \vec{\phi_g}, \tag{21}$$

where $\vec{\phi_g}$ is a gap interlinkage flux vector [11]. Another magnetizing current vector $\vec{i_g}$ can be defined as follows:

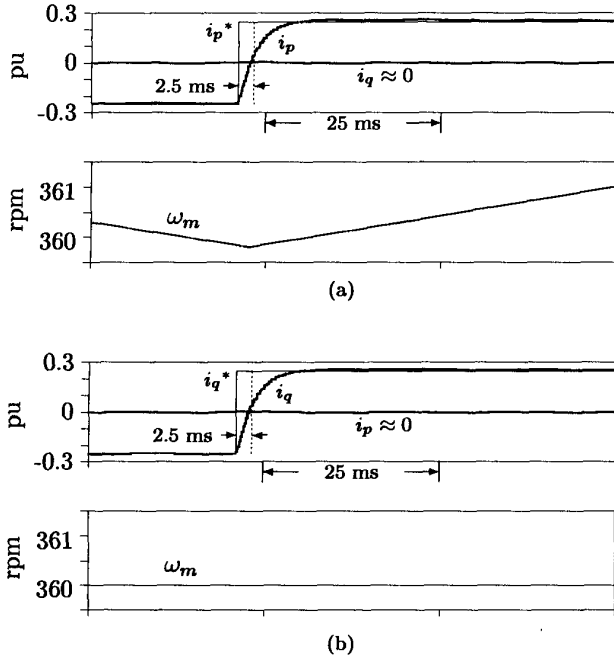$$\vec{\phi_g} = M\vec{i_g} = \vec{\phi_1} - l_1\vec{i_1}. \tag{22}$$

Fig. 9. Dynamic performance in case of considering the switching operation of the voltage-fed PWM inverter. (a) Step response of $i_p{}^*$ under $i_q{}^* = 0$. (b) Step response of $i_q{}^*$ under $i_p{}^* = 0$.

This suggests that $\vec{i}_g$ corresponds to the gap interlinkage flux vector. As a result, the following relationship exists among $\vec{i}_g$, $\vec{i}_0$ and $\vec{i}_1$:

$$\vec{i}_g = \frac{L_1}{M}\vec{i}_0 - \frac{l_1}{M}\vec{i}_1 \tag{23}$$

The theoretical discussion concludes that $\vec{\phi}_1$ depends only on $\vec{v}_1$, and $\vec{\phi}_g$ and $\vec{i}_g$ depend on $\vec{v}_1$ and $\vec{i}_i$. Note that $\vec{i}_1$ is not only the output vector but also the state vector of the control system.

D. Transient behavior of $\vec{i}_0$ and $\vec{i}_g$

The transient behavior of $\vec{i}_0$ and $\vec{i}_g$ is discussed below, taking into account the primary and secondary resistances r_1 and r_2. Fig. 8 shows simulated waveforms of voltage and current on the α-β coordinates, assuming that the amplitude of $\vec{v}_1$ is 1 pu. Here, the following step change in either $i_p{}^*$ or $i_q{}^*$ is intentionally made at the beginning of intervals II and III:

interval I	$i_p{}^* = 0$	$i_q{}^* = 0$
interval II	$i_p{}^* = 0$	$i_q{}^* = -0.35$
interval III	$i_p{}^* = 0.35$	$i_q{}^* = -0.35$

Note that the authors impose a constraint of $i_{\alpha2} = i_{\beta2} = 0$ during the steady state on interval II, in order to determine the values of $i_p{}^*$ $(= i_{\gamma1})$ and $i_q{}^*$ $(= i_{\delta1})$. As a result, the constraint produces the instantaneous active and reactive

references of $i_p{}^* = 0$ and $i_q{}^* = -0.35$ in interval II. Fig. 8 results in the following observations related to $\vec{i}_0$:

- The amplitude of $\vec{i}_0$ is held constant during intervals I, II and III, although the amplitude of $\vec{i}_g$ varies.
- The phase of $\vec{i}_0$ lags by 90° with respect to that of $\vec{v}_1$
- During interval I, $\vec{i}_0$ is supplied from the secondary because $\vec{i}_1 = 0$,
- During interval II, $\vec{i}_0$ is supplied from the primary because $\vec{i}_2 = 0$.

Thus, it is concluded that $\vec{i}_0$ is automatically supplied from the primary and/or the secondary, not only in the steady state but also in the transient state, so as to have a constant amplitude independent of i_p and i_q. In addition, $\vec{i}_g$ is not a directly-controllable variable because it is determined as a result of having controlled i_p and i_q.

V. DYNAMIC PERFORMANCE IN CASE OF CONSIDERING THE PWM INVERTER

Fig. 9 shows simulated waveforms in which the switching operation of the voltage-fed PWM inverter is taken into account. Here, the control system for i_p and i_q has a proportional-plus-integral (PI) controller, the time constant of which is set at $T_I = 100$ ms. The proportional gain is designed to be $K = 0.5$ [V/A], so that the time constant of i_p and i_q for a step change in $i_p{}^*$ and $i_q{}^*$ is $T = 2.5$ ms. The triangle-carrier frequency of the voltage-fed PWM inverter is 1 kHz, and the dc link voltage is 0.2 pu. The magnitude of the step change in $i_p{}^*$ and $i_q{}^*$ is set to be ±0.25 pu, so that the maximum output voltage of the inverter does not reach the saturation voltage, that is, the dc link voltage of 0.2 pu. If the magnitude of the step change is large enough for the control system to reach saturation, it would be impossible to evaluate the response inherent in the control system from the resulting response to the step change, because the saturation voltage would dominate the resulting response to the step change.

Fig. 9 exhibits that the time constant of i_p and i_q is 2.5 ms ($\omega_c = 400$ rad/s) which is equal to its design value, and that no cross-coupling occurs between i_p and i_q. The rotor speed of the induction machine, ω_m varies in Fig. 9 (a), whereas it is held constant at 360 rpm in Fig. 9 (b) because $i_p = 0$.

VI. CONCLUSION

This paper has described the control strategy and dynamic performance of a flywheel energy storage system based on a doubly-fed induction machine for power conditioning. The validity of the theory developed in this paper is verified by computer simulation using EMTDC. This paper can be summarized as follows:

- A new control strategy based on the combination of vector control and decoupling control has been proposed, which is characterized by constituting direct feedback loops of i_p and i_q.
- The resulting response to a step change in $i_p{}^*$ or $i_q{}^*$ is a first-order system with a time constant of $T = l/K$. Here, l is a leakage inductance given by (4), and K is a proportional gain.

38

- The magnetizing current corresponding to the primary interlinkage flux is automatically supplied from the primary and/or the secondary, not only in the steady state but also in the transient state, and the amplitude of the magnetizing current is held constant, independent of i_p and i_q.
- The magnetizing current corresponding to the gap interlinkage flux is not a directly-controllable variable because it is determined as a result of having controlled i_p and i_q.

The flywheel energy storage system based on a doubly-fed induction machine is expected to be used exclusively as a versatile power conditioner, in particular, being capable of repetitively absorbing and releasing electric energy for a short period of time less than a minute.

VII. ACKNOWLEDGMENT

The authors would like to thank Toshiba Corporation for providing helpful and valuable information of the 200-MJ flywheel energy storage system. They would also like to thank Prof. Scott Gardner at the Okayama University for his English language editing.

REFERENCES

[1] H. Sato, T. Sueno, T. Toyama, M. Mikawa, T. Toda, "High-accutacy magnet power supply for proton synchrotron by repetitive control," in *Proceedings of the 1991 IEEE/PESC*, pp. 812-816, 1991.

[2] Loren H. Walker, "10-MW GTO Converter for Battery Peaking Service," *IEEE Trans. Ind. Appl.*, vol. 26, no. 1, pp. 63-72, 1990.

[3] I. D. Hassan, R. M. Bucci, K. T. Swe, "400 MW SMES power conditioning system: Part I–Performance requirements and configuration," in *Proceedings of the 1991 IEEE/PESC*, pp. 338-344.

[4] I. D. Hassan, R. M. Bucci, K. T. Swe, "400 MW SMES power conditioning system: Part II–Operation and dynamic performance," in *Proceedings of the 1991 IEEE/PESC*, pp. 345-353.

[5] T. Nohara, H. Senaha, T. Kageyama and T. Tsukada, "Successful commercial operation of doubly-fed adjustable-speed flywheel generating system," in *Proceedings of the CIGRE/IEE Japan Joint Colloquium on Rotating Electric Machinery Life Extension, Availability Improvement, and Development of New Machinery*, (2-2), pp. 1-6, 1997.

[6] W. Leonhard, "Control of electric drives," Springer-Verlag, pp.244-259, 1985.

[7] M. Yamamoto, and O. Motoyoshi, "Active and reactive power control for a doubly-fed wound-rotor induction generator," *IEEE Trans. Power Electronics*, vol. 6, no. 4, pp. 624-629, 1991.

[8] C. Brune, R. Spée, and A.K. Wallace "Experimental evaluation of a variable-speed, doubly-fed wind-power generation system," in *Proceedings of the 1993 IEEE/IAS Annual Meeting*, pp. 480-487.

[9] S. Bhowmik, R. Spée, and J.H.L. Enslin, "Performance optimization for doubly-fed wind power generation systems," in *Proceedings of the 1998 IEEE/IAS Annual Meeting*, pp. 2387-2394.

[10] H. Akagi, Y. Kanazawa and A. Nabae, "Instantaneous reactive power compensators comprising switching devices without energy storage components," *IEEE Trans. Ind. Appl.*, vol. 20, no. 3, pp. 625-630, 1984.

[11] A. Nabae, K. Otsuka, H. Uchino, and R. Kurosawa, "An approach to flux control of induction motors operated with variable frequency power supply," *IEEE Trans. Ind. Appl.*, vol. 16, no. 2, pp. 342-348, 1980.

[12] S. Ogasawara, H. Akagi, and A. Nabae, "The generalized theory of indirect vector control for ac machines," *IEEE Trans. Ind. Appl.*, vol. 24, no. 3, pp. 470-478, 1988.